ELSEVIER

Journal of Structural Geology 28 (2006) 268–283

JOURNAL OF STRUCTURAL GEOLOGY

www.elsevier.com/locate/jsg

Geometry, kinematics, and landscape characteristics of an active transtension zone, Karakoram fault system, Southwest Tibet

Michael A. Murphy *, W. Paul Burgess [1]

Department of Geosciences, University of Houston, Houston, TX 77204-5007, USA

Received 13 April 2005; received in revised form 4 October 2005; accepted 5 October 2005
Available online 15 December 2005

Abstract

We investigate the style of active transtensional deformation and characteristics of the landscape along the southern segment of the Karakoram fault system through field mapping, structural analysis, and examination of digital topography (SRTM, ASTER), multi-spectral (ASTER, Landsat 7+), and panchromatic (Corona photography) imagery. Our data suggests that wrench-dominated transtension is occurring within a 90-km-wide zone; simple shear within the zone is accommodated by right-lateral R and P shears as well as left-lateral R′ shears, vertical shortening is accommodated by ~north-striking extensional shear zones and horizontal shortening is accommodated by ~east–west-trending transtension-related corrugations. Drainage divides strike at high angles and subparallel to the transtension zone. Those that strike at high angles to the zone can be explained by movement along north-striking extensional fault systems, while the geometry of drainage divides subparallel to the zone are consistent with uplift of corrugations as well as rapid uplift of mountain ranges by normal-right-slip faulting.
© 2006 Elsevier Ltd. All rights reserved.

Keywords: Strike-slip faulting; Transtension; Himalaya; Tibetan plateau

1. Introduction

Central to assessing the deformation behavior of continental lithosphere is a complete description of the bulk strain in theorized intracontinental plate boundaries. In various tectonic settings worldwide it has been shown that deformation within the continents is distributed across wide zones and that the motion is commonly oblique to the boundaries resulting in transpressional or transtensional deformation, for example, the Walker Lane belt (e.g. Oldow et al., 2001), Central Alps (e.g. Dewey et al., 1998), and Alpine fault zone (e.g. Norris et al., 1990). Sophisticated kinematic models due to oblique motion (transpression and transtension) have been developed (e.g. Tikoff and Teyssier, 1994; Fossen and Tikoff, 1998; Dewey, 2002) and have held up to extensive field-based structural studies. What has received considerably less attention is examination of landscape characteristics and how they compare with predictions made by transpression and transtension models.

Herein, we present geologic and geomorphologic observations from southwest Tibet and northwest Nepal, in the vicinity of Mt. Kailas. We assess the relationship between active deformation along the Karakoram fault, topography, and drainage patterns and show that they support the view that the landscape can be explained by wrench-dominated transtension, distributed across a 90-km-wide zone.

The central and southern segment of the Karakoram fault system is broadly situated between two structurally distinct domains within the Tibet–Himalayan collision zone. To its east is the Tibetan plateau, which is actively undergoing conjugate strike-slip faulting and east–west extension (Rothery and Drury, 1984; Armijo et al., 1989; Taylor et al., 2003; Kapp and Guynn, 2004), while to its west is the Himalayan fold-thrust belt, which is dominated by thrusting perpendicular to the trace of the Himalayan front. This dramatic change in deformation style across the fault as well as its regional extent and long life-span has attracted a great deal of attention on the role of this fault in accommodating the relative motion between the Tibetan plateau and Himalayas (e.g. Armijo et al., 1989;

* Corresponding author. Tel.: +1 713 743 3413; fax: +1 713 748 7906.
E-mail addresses: mmurphy@mail.uh.edu (M.A. Murphy), wburgess@ucla.edu (W.P. Burgess).
[1] Now at: Department of Earth and Space Sciences, University of California, Los Angeles, 595 Charles E. Young Dr. E., Los Angeles, CA 90095-1567, USA.

0191-8141/$ - see front matter © 2006 Elsevier Ltd. All rights reserved.
doi:10.1016/j.jsg.2005.10.009

Avouac and Tapponnier, 1993; Searle, 1996; Yin and Harrison, 2000; Replumaz and Tapponnier, 2003; Taylor et al., 2003; Murphy and Copeland, 2005).

Transtensional deformation has been described along the Karakoram fault at several localities (Armijo et al., 1989; Ratschbacher et al., 1994; Searle, 1996; Searle et al., 1998; Murphy et al., 2000; Kapp et al., 2003; Murphy and Copeland, 2005) and is predicted by GPS-derived velocity models of the Tibet–Himalaya orogen (Larson et al., 1999; Wang et al., 2001; Zhang et al., 2004; Jade et al., 2004). The Karakoram fault system is widely considered to be a discrete narrow fault zone. However, south of 32°N the fault system appears to be more

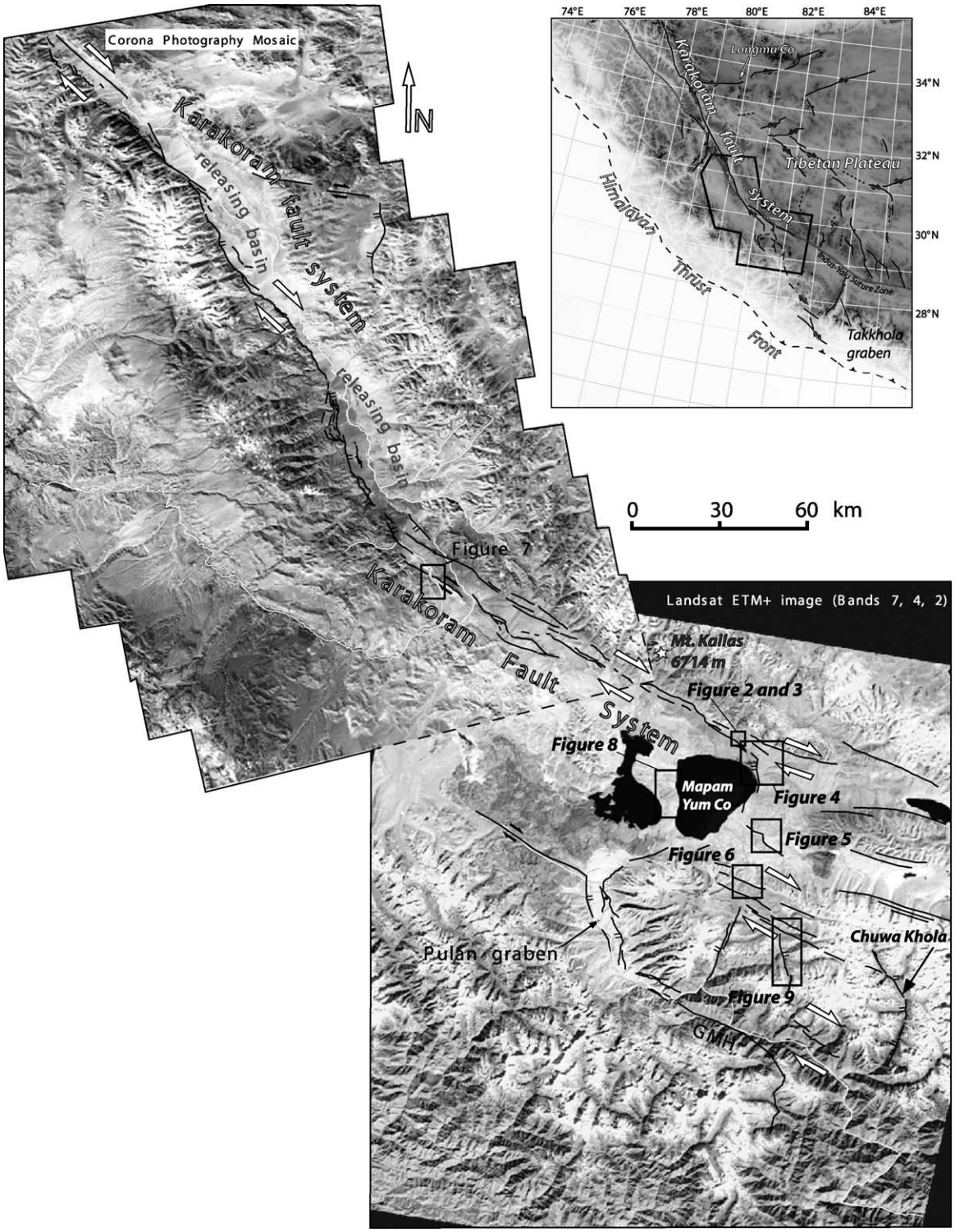

Fig. 1. Active fault map of the southern segment of the Karakoram fault system. Base map is a mosaic of Corona photography scenes in the north and Landsat ETM+ in the south. Black boxes indicate the location of sites investigated in the field and using satellite imagery. Inset shows the location of the Karakoram fault system in the Tibet–Himalayan orogen. GMH, Gurla Mandhata–Humla fault system.

complex, consisting of several structures with a variety of orientations (Ni and Barazangi, 1984; Armijo et al., 1989; Ratschbacher et al., 1994; Zhang et al., 2000; Lacassin et al., 2004; Murphy and Copeland, 2005; this study) (Fig. 1). How these structures actively accommodate the bulk strain within this portion of the Karakoram fault system is explored in this paper.

2. Recent faulting in the Mt. Kailas area

2.1. Satellite imagery interpretation

2.1.1. North side of Mapam Yum Co

The main trace of the Karakoram fault strikes ~N40W following the south side of the Gangdese range (Figs. 2 and 3).

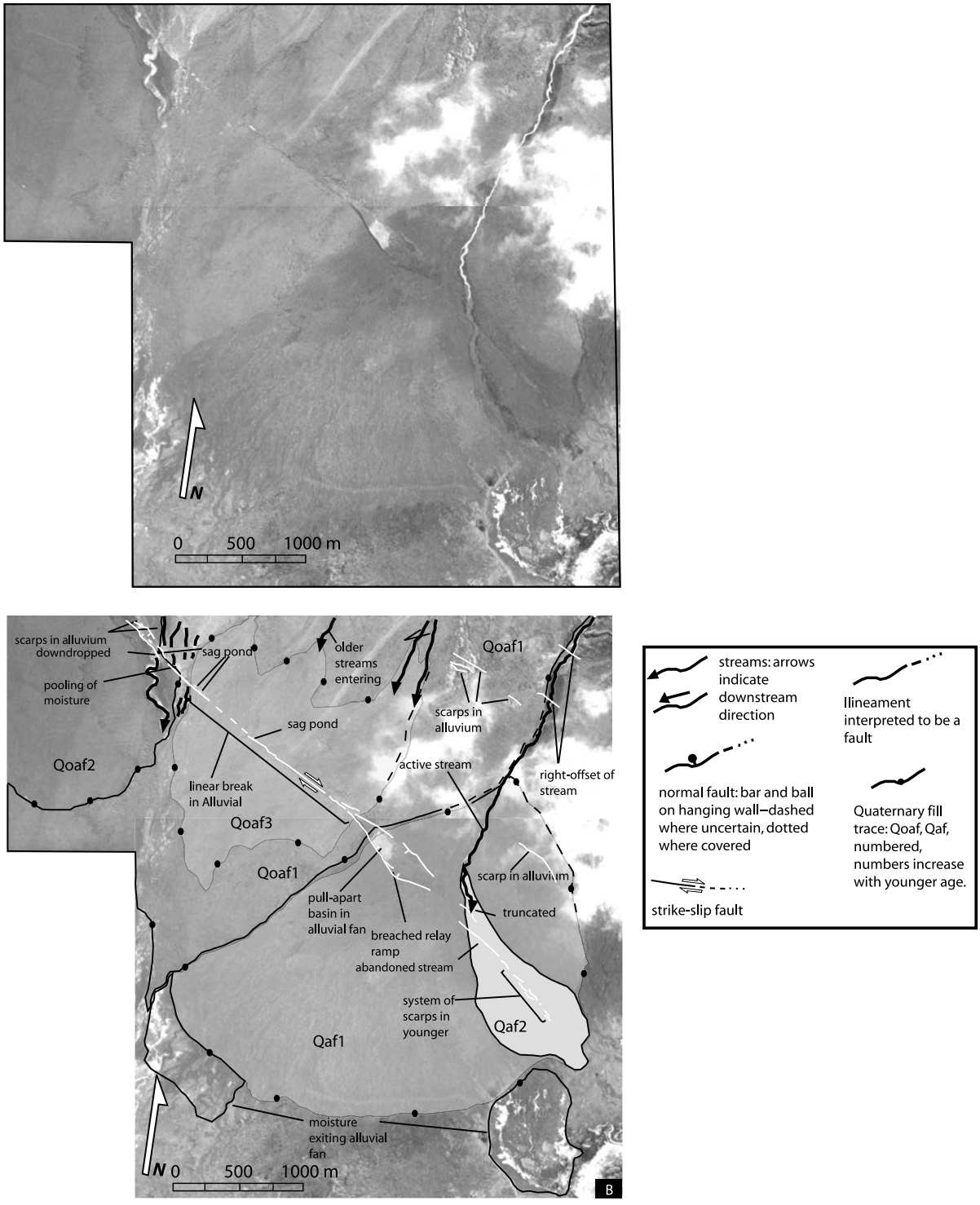

Fig. 2. (A) Mosaiced CORONA imagery showing a fault scarp along the Karakoram fault just north of Mapam Yum Co. (B) Interpretation of (A). See Fig. 1 for location.

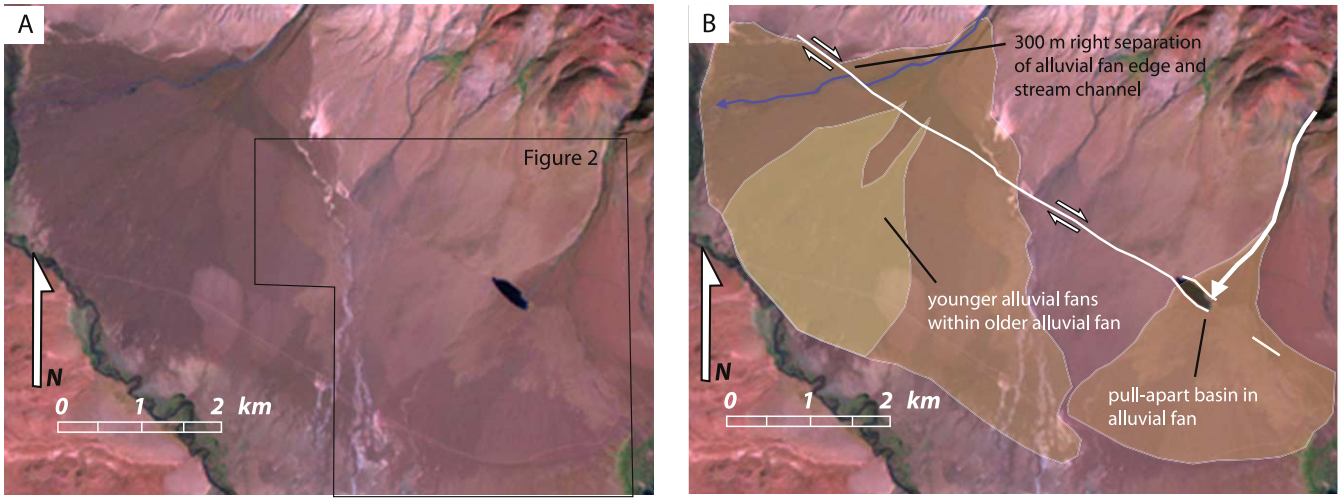

Fig. 3. Landsat 7+ image (bands 743) of the region north of Mapam Yum Co.

This area is expressed by an ~4-km-long scarp that correlates to other scarps along strike for several tens of kilometers (Fig. 1). The scarp cuts several alluvial fans (Figs. 2 and 3). We use alluvial fans as indicators of active faulting to establish (1) the location of their youngest deposited sediments and (2) the character of the stream responsible for sedimentation as it enters the alluvial fan (Keller and Pinter, 2002). Sediment in this area is transported first to the southwest and then due southeast into Mapam Yum Co via two prominent streams, one of which incises the upper portion of the right-most alluvial fan in Fig. 2. This observation combined with the interpretation that the most recent alluvial deposition unit is found near the fanhead indicates that the uplift of the range-front is faster than the rate of down-cutting of the stream channel. These fans display a discolored surface compared with the lithology surrounding them (Figs. 2 and 3). In CORONA imagery, darker colors indicate a lower albedo of the surface, which may provide a first-order constraint on either the age or lithology of a surface. ASTER and Landsat 7+ data narrows this interpretation. The 312 (RGB) band combination of ASTER data and 743 (RGB) band combination of Landsat 7+ data reveal that the alluvial fans consist of purple and dark pink colors, respectively, which indicates a higher level of moisture in the alluvial fans compared with adjacent lithology. Thus these fans are recent in age, and offset of them reflects recent faulting.

A clear lineament cuts across the fans (Figs. 2 and 3) and parallels the mountain front. Geomorphic features of the right-most alluvial fan broadly define the location of an active strand of the Karakoram fault system. Small bends and relay ramps in the fault suggest that the fault system experiences local changes in orientation along-strike, characteristic of a small right-stepping style of geometry (Figs. 2 and 3). The general character of the upper portion of the right-most alluvial fan provides compelling evidence for a semi-continuous fault scarp that strikes roughly parallel to the trend of the mountain front and can be traced for a distance of slightly more than 4 km. This fault is interpreted to accommodate right-lateral strike-slip. From northwest to southeast the major geomorphic features defining right-lateral strike slip are: stream pooling, sag ponds, a pull-apart basin within the alluvial fan, and stream channel offset and truncation (Fig. 2). Present throughout the north side of Mapam Yum Co are numerous <100–~500-m-long scarps in all types of alluvium (Fig. 2). The distribution of these scarps indicates that active deformation along the front of the Gangdese range is occurring in a zone slightly wider than ~2 km and has occurred at least since the deposition of the oldest alluvial sediments. These scarps are interpreted to be only a few meters high based on the minimal amounts of scarp being either lit up by sunlight or alternatively casting shadows as visible in the CORONA imagery (Fig. 2).

The pull-apart basin, and offset and truncation of the right-most active stream channel illustrate a change in orientation of the active fault segment that is characteristic of right-stepping right-lateral strike-slip faulting. The pull-apart basin and the truncation of the stream indicate that active right-slip faults display right steps along strike. Evidence supporting a normal component of slip along right-slip faults is found in the truncation of the prominent stream channel to the right of the pull-apart basin. North of the scarp the stream channel is narrow (<100 m) and below the scarp the stream channel flares to a larger width (Fig. 2). This observation may be explained by a southward-dipping fault with the south side downthrown.

Especially relevant to the interpretation that active right-lateral strike-slip faulting has a component of normal dip-slip is illustrated by the presence of small younger alluvial fans developing on the left alluvial fan in Fig. 3. We interpret these fans developed due to south-side down relative motion along a south dipping fault scarp. The prominent right-lateral offset of the edge of the leftmost fan and stream channel show a ~300 m right separation.

2.1.2. Northeast corner of Mapam Yum Co (northern releasing bend)

Fig. 4 is an ASTER scene (bands 321) of the northeast corner of Mapam Yum Co. This area consists of marshy terrain bordering the lake on its west side, and drier, alluvial terrain on

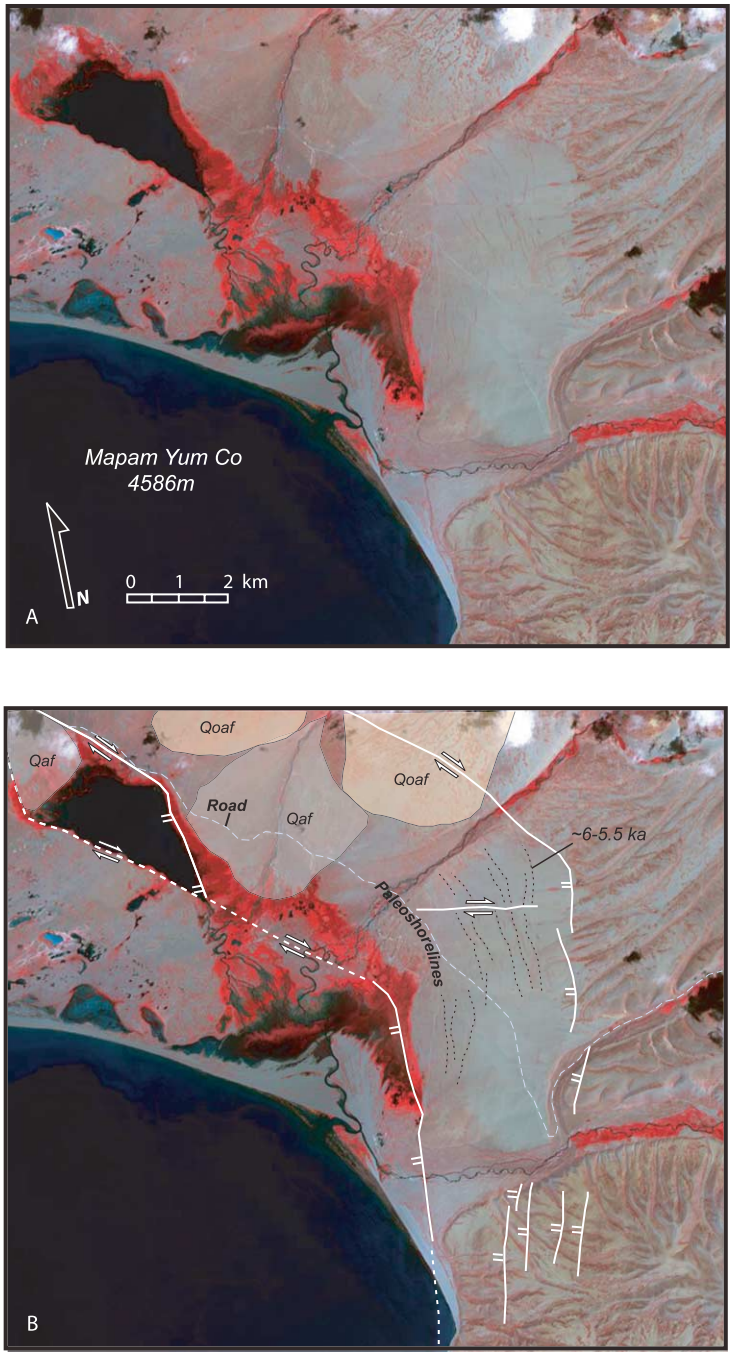

Fig. 4. (A) ASTER scene (bands 321) of the northeast corner of Mapam Yum Co. (B) Interpretation of active faults at the northeast corner of Mapam Yum Co. Landforms include offset paleoshorelines; date in top right is inferred from ages for the oldest documented paleoshorelines Longmu Co (Avouac et al., 1996). See Fig. 1 for location and text for discussion.

its eastern side. Several geomorphic indicators of active faulting are present in this location. The following relationships were observed around the eastern perimeter of Mapam Yum Co: (1) N30–40°W striking active faults displaying right-lateral separations cut the oldest alluvial fans; (2) these faults link with north-striking, west-facing fault scarps that suggest west-side down motion based on topographic changes across the scarp; (3) shallow lakes and regions of high moisture content display straight borders that parallel fault scarps; and (4) this system of faults cut paeloshorelines of Mapam Yum Co. These relationships broadly define two linked normal fault and right-slip fault systems, a northern system and a southern system. Both systems merge in the south along the eastern boundary of Mapam Yum Co. We interpret the shallow lake represents a more involved version of the pull-apart basin described in the previous section. Although active right-slip faults extend eastward past Mapam Yum Co as described by Lacassin et al. (2004), we interpret that most of the active

right-slip faults along the southern flank of the Gangdese shan link with normal faults that roughly coincide with the eastern boundary of Mapam Yum Co.

2.1.3. East of Mapam Yum Co

Fig. 5 is a CORONA image of a region ~20 km due south of the last study area (Fig. 4). The geology is characterized by bedrock outcrop with some alluvial sediment in the southeast corner (Fig. 5). Prominent indicators of faulting in the southern half of the location from west to east include: (1) flatirons in the center left of the image that strike N45W; (2) a disrupted stream channel causing stream pooling southeast of the flatirons; and (3) abandoned stream channels in the southern portion of the study area (Fig. 5). Other geomorphic indicators of active faulting include abundant scarps of two types: one set that strikes between N70W and N40W and another set that strikes ~north–south. Fault scarp geometry suggests the presence of small pull-apart basins. Disrupted/offset stream channels display a right-lateral sense of motion with a component of south-side down motion.

Of particular interest is the broad zone of incised alluvial terraces in the southeast corner of this study area. The main river flows west through an alluvial area, then north parallel to a topographically higher area, and then northwest cutting through bedrock. We interpret the alluvial area to represent a local topographic low created by a releasing bend along a right-slip fault. This sense of motion is also based on the interpretation that strath and fill terraces bracket the course of the river proximal to the point in the middle of study area, where the river again enters a channel incised into bedrock.

2.1.4. Southeast of Mapam Yum Co (Tibet–Nepal border)

Fig. 6 is a CORONA image of a region situated ~40 km southeast of Mapam Yum Co (Figs. 4 and 5). This region consists of glacial moraines in its northwest corner and alluvium throughout the rest of the location (Fig. 6). Scarps showing right-lateral offset of geomorphic features vary in length from <1 to >6 km and strike between N60W and N40W (Fig. 6). The fault scarps are all southwest facing with the north side topographically higher. This suggests a component of normal dip-slip motion along active right-slip faults.

In the central part of this study area several large river channels have very small drainage basins. These drainage basins are bounded on their southern sides by southwest facing fault scarps. We interpret that these drainage basins were

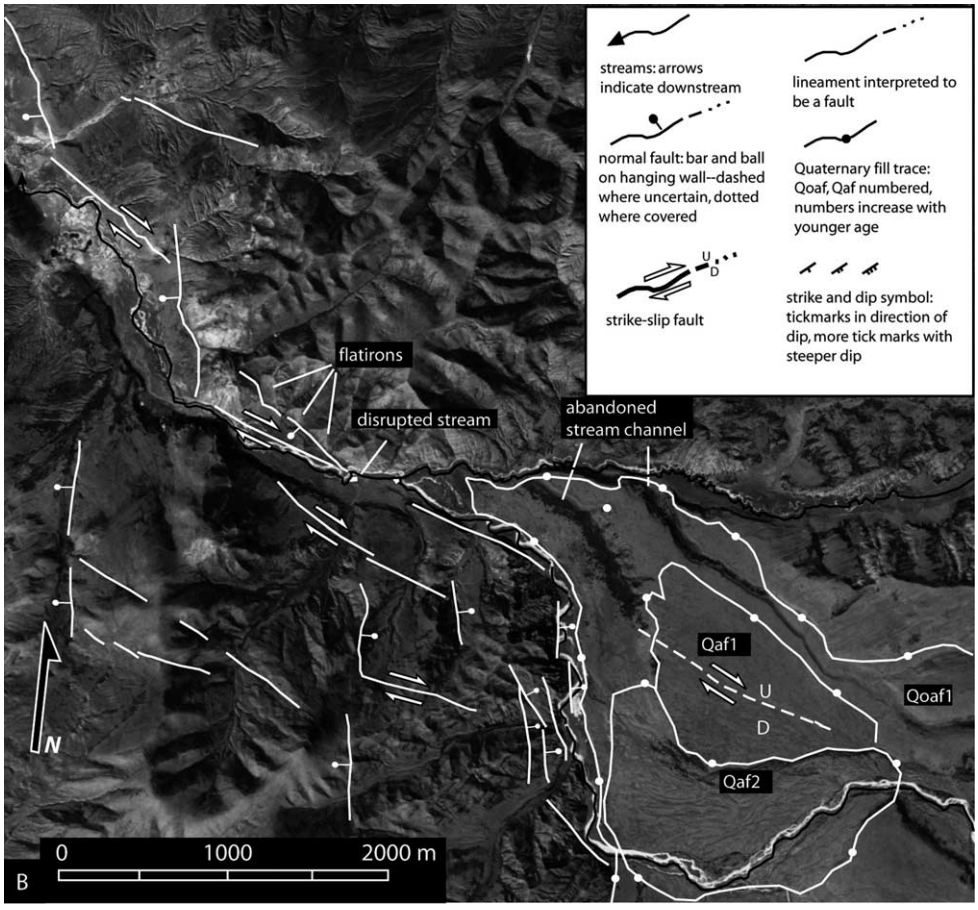

Fig. 5. CORONA satellite imagery of geomorphic features and interpreted active faults east of Mapam Yum Co. Exposed bedrock is visible in this image, except for the lower right corner, which consists of fluvial sediments deposited by the northwest flowing stream. Thick white lines with arrows are streams with downstream direction indicated. Prominent geomorphic indicators of faulting include scarps cutting alluvial fans, a pull-apart basin forming in an alluvial fan, and several right-laterally offset streams. See Fig. 1 for location and text for discussion.

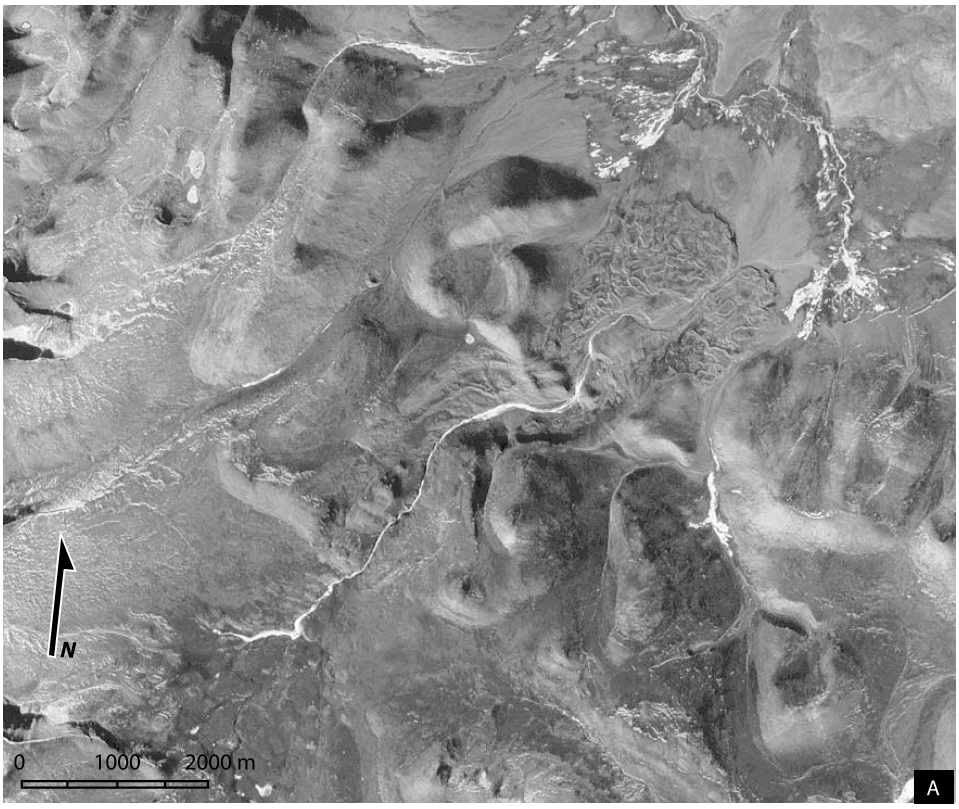

Fig. 6. CORONA satellite imagery of geomorphic features and interpreted active faults southeast of Mapam Yum Co along the Tibet–Nepal border. Arrows indicate sense of movement along structures. Thick black lines with arrows indicate active streams and downstream direction. Thin white lines with arrows indicate abandoned stream channels and downstream direction. See Fig. 1 for location and text for discussion.

originally much larger and that these faults have decreased their size. Two faults strike ~east–west. Assuming the right-slip faults reflect the trend of the principal displacement zone (N60W), then east–west faults may represent P-shears (the incident angle between these two fault types is 20–30°; Fig. 6). This system of fault continues eastward along the northern flank of the Gurla Mandhata metamorphic core complex as well as another core complex to the north. As discussed later, offset geomorphic features and stream profile characteristics suggest that the faults flanking the Gurla Mandhata metamorphic core complex accommodate both right-slip and top-to-north dip-slip motion.

2.2. Field mapping

Structural mapping along the Karakoram fault was conducted at several localities in southwest Tibet and northwest Nepal at a scale of 1:100,000 and 1:50,000, respectively (Fig. 1). Below, we present field mapping, fault-slip, and fracture data from field localities along the Karakoram fault. All data presented are from late brittle structures since the region has had a long deformation history. We measured faults that the have an outcrop length >1 m, and display some sense-of-shear indicator. Shear-direction indicators used for faults include striae, grooves, slickenlines, mineral fibers, en échelon tension gashes, and Riedel shears. We use the term shear fracture to denote a fracture with <1 cm of slip and the term fault to indicate >1 cm of offset.

2.2.1. Menci area

The town of Menci lies along one of the southern branches of the Karakoram fault system (Figs. 1 and 7). Along most of its length, the fault strikes N50W and dips 85–65°S and cuts Ordovician phyllite and quartzite units as well as upper Tertiary boulder cobble gravel conglomerates. Three main faults were recognized south and west of Menci, two northwest-striking right-slip faults and a north-striking west-dipping normal fault. All faults are younger than the upper Tertiary conglomerates, which may be as young as Pliocene based on correlations to the Zada Formation (Cheng and Xu, 1987). They typically occur as a $\leq$3-m-thick gouge and calaclasite zone. Fault surfaces within the fault zones display grooves and slickenlines and commonly have centimeter scale Riedel shears adjacent to them. The mean orientation of both the northern and southern right-slip faults is N50W/75SW. Slip directions calculated from shear sense indicators trend between N40W and N60W and plunge $<15°$. The intervening west-dipping normal fault has a mean orientation of N/65W. Slip directions on the fault show nearly pure dip-slip motion towards the west. Offset of the Tcg1–Opq contact requires approximately 250 m of net slip on the fault. Smaller offset conjugate normal faults adjacent to the main fault have a mean

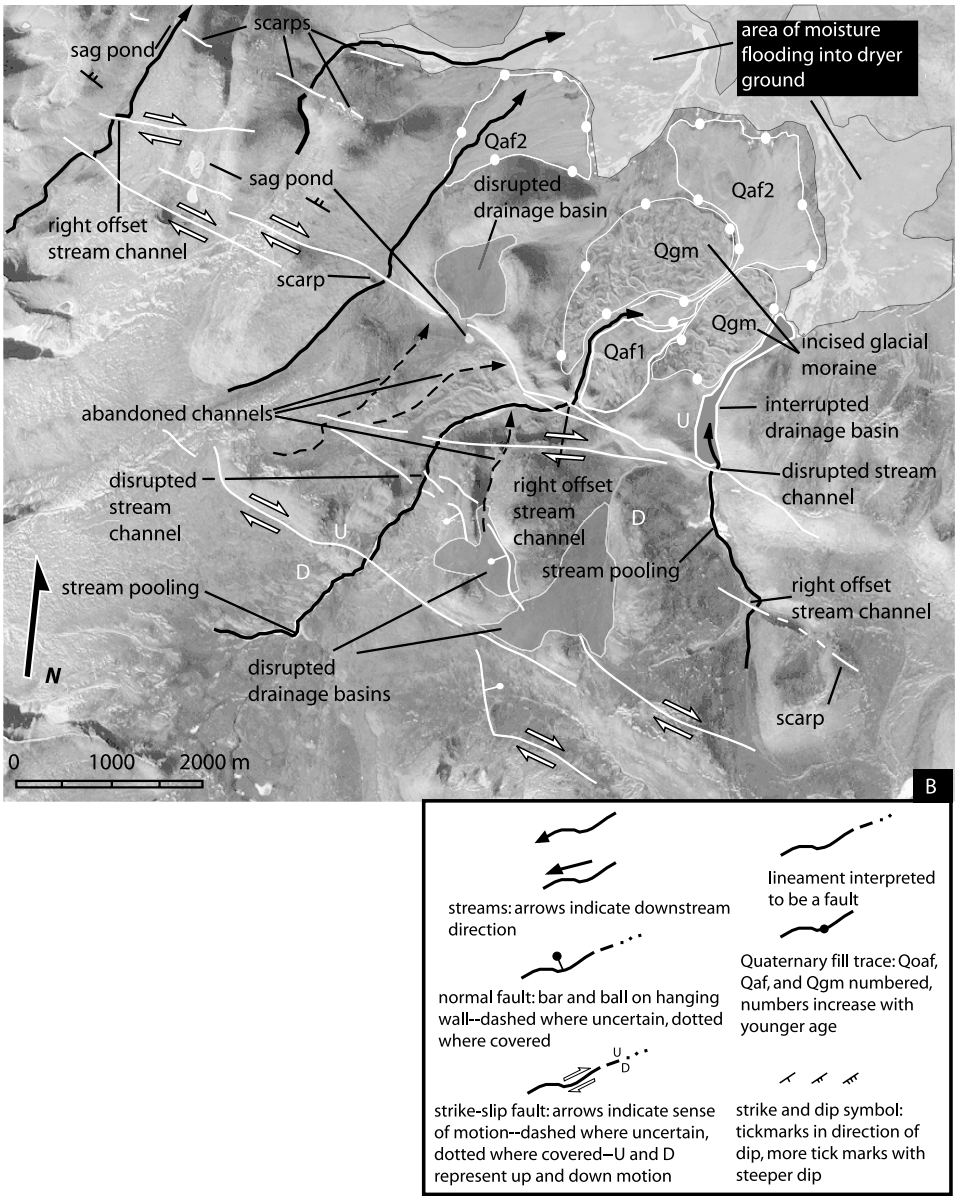

Fig. 6 (*continued*)

orientation of N5W/56NE. East and west dipping normal faults share an acute angle of 59° between them and are interpreted to be conjugate to one another. Although intersections between the right-slip faults and normal faults were not exposed, we interpret the northern right-slip fault is linked to the southern right-slip fault based on their similar deformation style and relative age.

2.2.2. Mapam Yum Co

Mapam Yum Co lies in a large, internally drained basin immediately south of Mt. Kailas and due north of Gurla Mandhata (Fig. 1). The active Karakoram fault strikes northwest along the northern side of Mapam Yum Co. Along the northwestern side of Mapam Yum Co, two main fault sets were recognized, northwest-striking right-slip faults, and north-striking normal faults (Fig. 8) (Murphy et al., 2002). Both fault sets cut Paleozoic metasedimentary rocks and Tertiary boulder cobble conglomerates. Faults typically occur as $\leq$10-cm-wide zones of cataclasite and are commonly polished. The mean orientation of right-slip faults is N53W/77SW. Slip directions vary from N47W to N58W and plunge $\leq$15°. The mean orientation of normal faults is N/65W. Slip directions on these faults are due west. At one locality a hard link was observed between a right-slip fault and normal fault (Fig. 8) indicating a kinematic link between the two. Slip directions on normal faults coincide with the intersection line between right-slip faults and normal faults consistent with these faults being kinematically linked.

2.2.3. Takchhe Valley

Takchhe valley is a north–south-trending glacially carved valley and lies south of a recent right-slip fault system (Fig. 9). The valley parallels a north-striking normal fault system that changes dip direction along strike. Fracture data from the

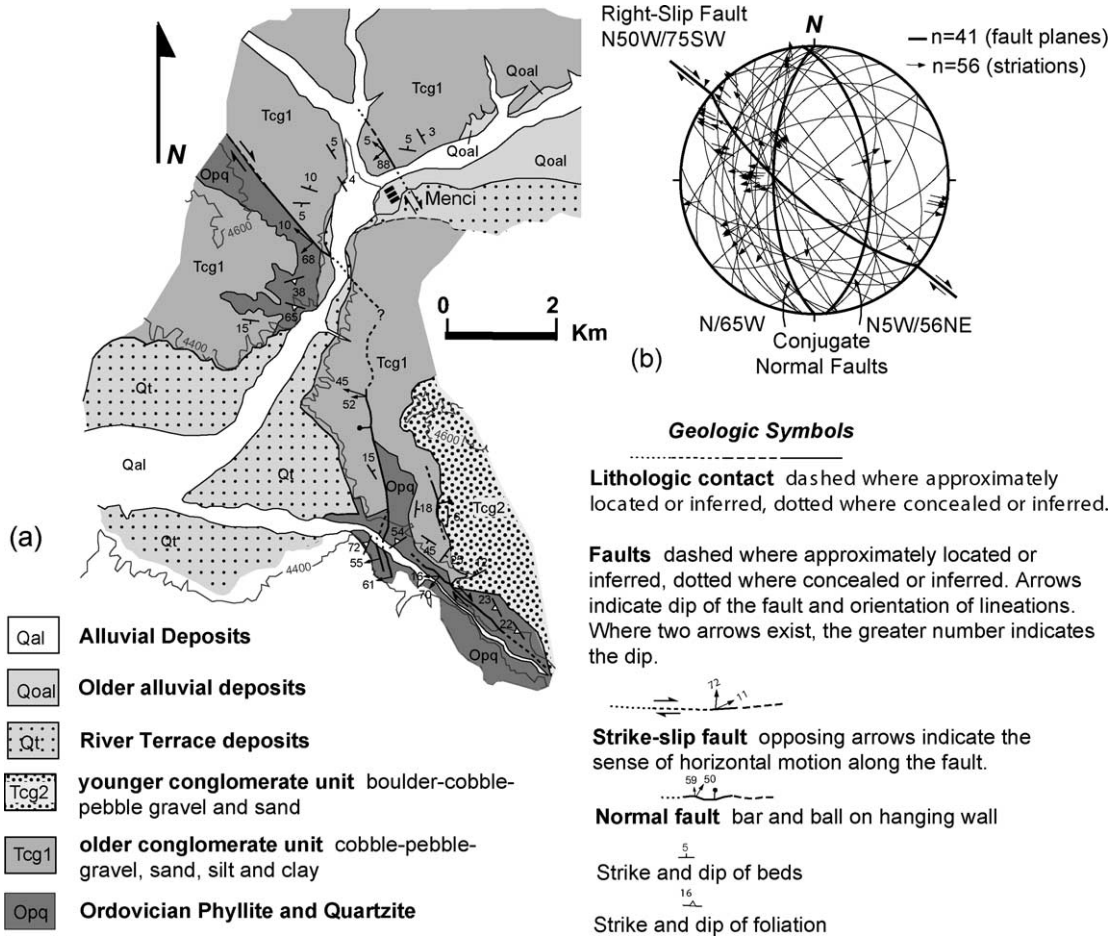

Fig. 7. Geologic map and structural data from the Menci area.

northern Takchhe valley show four common fracture orientations, F1, F2, F3, and F4 (Fig. 9). F1 is a steeply dipping northwest-striking set of shear fractures and has a maximum density pole of N42E/09. Small offsets observed along F1 fractures indicate right-slip motion. F2 is a subvertical set of east–northeast-striking shear fractures. F2 has a maximum density pole of N11W/1.5 and also displays right-slip offsets. F3 fractures are steeply dipping to the northwest and strike north–northeast. F3 fractures have a maximum density pole of S55E/24 and display left-slip offsets. F4 fractures are subvertical and strike north. F4 fractures are open or Mode 1 fractures and are commonly filled with quartz.

North of Takchhe valley, several west–northwest-striking faults cut across the landscape and display geomorphic features that suggest a significant component of right-slip (Fig. 9). Unfortunately, no shear-sense indicators were preserved on these young faults. However, the faults strike parallel to the Gurla Mandhata–Humla fault approximately 20 km south of Takchhe (Murphy and Copeland, 2005). The Gurla Mandhata–Humla fault strikes WNW and dips moderately to the south. Fault-slip data indicates dominantly right-slip motion along the Gurla Mandhata–Humla fault with a smaller component of normal dip-slip motion (Fig. 1). We correlate faults in the Takchhe valley to the Gurla Mandhata–Humla fault, and interpret that fractures in the northern Takchhe valley are associated with dominantly right-slip motion on west–northwest-striking faults (Fig. 9). In this scenario, F1, F2, and F3 fractures are interpreted as R, P, and R′ shears, respectively. F1, F2, and F3 are at angles of 24°, −31°, and 80°, respectively, to a principle displacement zone striking N41W/85SW.

Takchhe valley is bounded on its eastside by moderately dipping north–northeast-striking faults. The fault zone is characterized by a 1–5-m-wide zone of cataclasite composed of striated boulder to cobble size angular clasts of mylonitic gneiss that is part of the Greater Himalayan complex. Shear sense indicators indicate the last phase of motion was dominantly normal dip-slip (Fig. 9). Both synthetic and antithetic faults are present in the fault zone. Synthetic faults share similar orientations to F3 fractures, which we interpret as R′ shears.

2.2.4. Chuwa khola

Chuwa khola is a north–south-trending glacial valley located in the southeastern corner of the study area (Fig. 1). A geologic map of Chuwa khola is shown in Murphy and Copeland (2005). Chuwa khola lies south of the eastern end of west–northwest-striking recently active right-slip fault system (Fig. 1). The valley displays triangular facets on its eastern and western margins. Our mapping shows that triangular facets

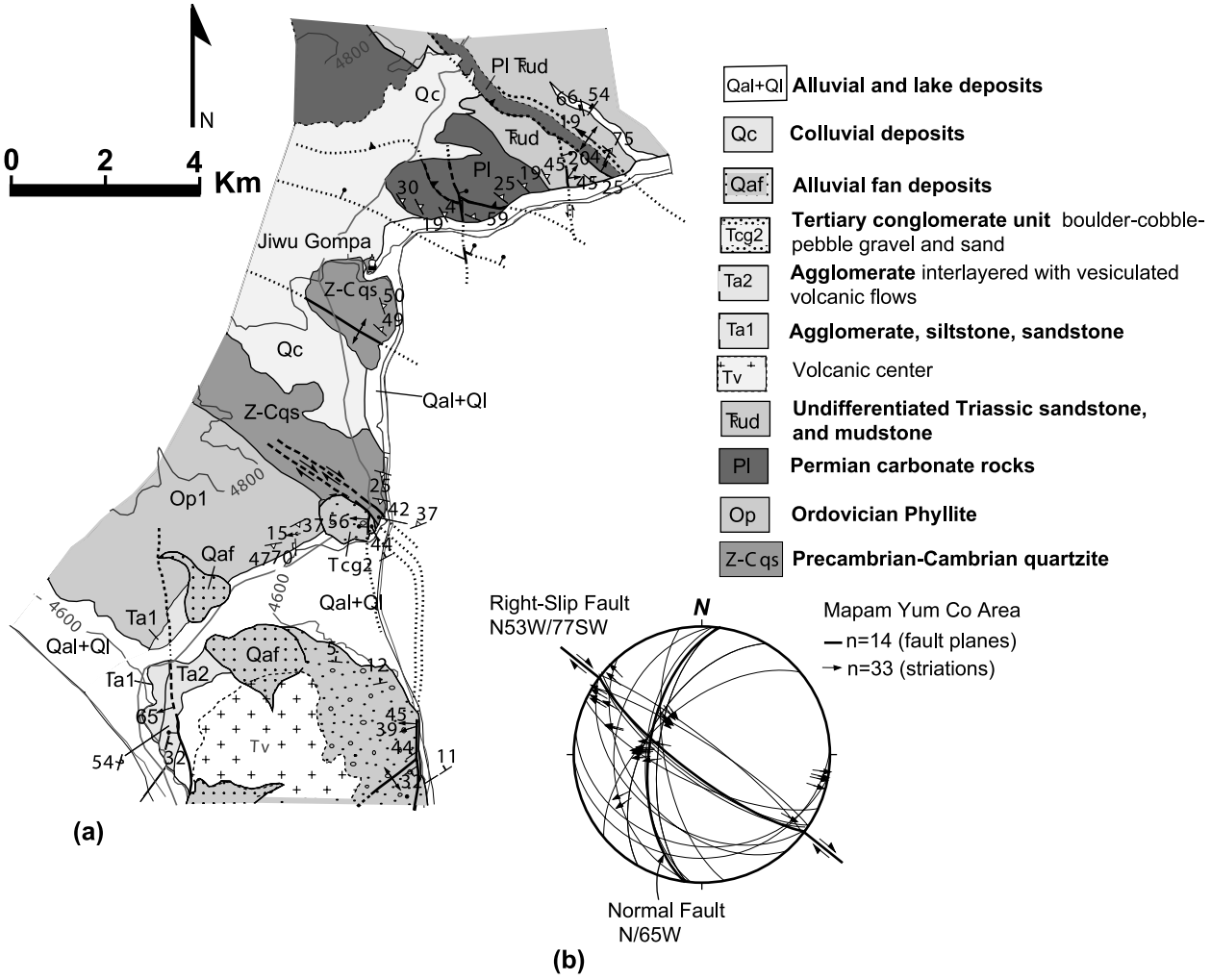

Fig. 8. Geologic map and structural data from the western margin of Mapam Yum Co.

developed due to slip on normal faults bounding Chuwa khola. Although rocks on both sides of the valley can be correlated, the intensity of brittle deformation is highest on the eastern margin. The trace of the main fault along the eastern margin can be followed for the entire length of Chuwa khola and strikes north–northwest and dips moderately towards the west. The fault cuts quartzofeldspathic mylonitic gneiss and schist that is folded about east–west-trending fold axes. The fault zone is approximately 1–5 m wide. It consists of monolithologic fault breccia that contains striated boulder to gravel size clasts. Fault-slip data from faults within the fault zone of the main fault indicate an average slip direction toward S75W (Fig. 10). Fault geometries and shear sense show well developed P and R shears within a principle displacement zone oriented N38W/42SW. P and R shears have a mean orientation of N46W/27SW and N30W/73SW, respectively. Another common fault orientation is N17E/63NW and displays variable slip directions from left-slip to pure dip-slip (Fig. 10). Within the central portion of Chuwa khola these faults parallel the main trace of the master fault, suggesting that the main fault exploits these faults to link with adjacent NW-striking segments.

3. Discussion

The observations presented in this paper show that active deformation along the Karakoram fault between 81°E and 82°E is accommodated by many discontinuous northwest-striking right-slip faults and north-striking extensional structures (Fig. 11). The longest system of normal faults lies along the eastern side of Mapam Yum Co and is interpreted as a stepover structure that feeds slip into a system of northwest-striking right-slip faults. Our structural observations show that most strike-slip faults have a minor normal dip-slip component (Figs. 2, 6 and 8). The strike of the Mt. Kailas reach of the Karakoram fault is ~N60W. Faults in this zone commonly dip steeply to the southwest. The mean slip direction of brittle strike-slip faults in the Menci is N65W and plot close to the intersection line between strike-slip faults and normal faults implying the two are kinematically linked. Moreover, the rake of striations indicates that the dip-slip component on individual strike-slip faults is between 15 and 60% of the net slip.

At all localities investigated the orientation of extensional stepover structures are at high angles to right-slip faults, varying between 80 and 42°. Eastward from the town of Menci

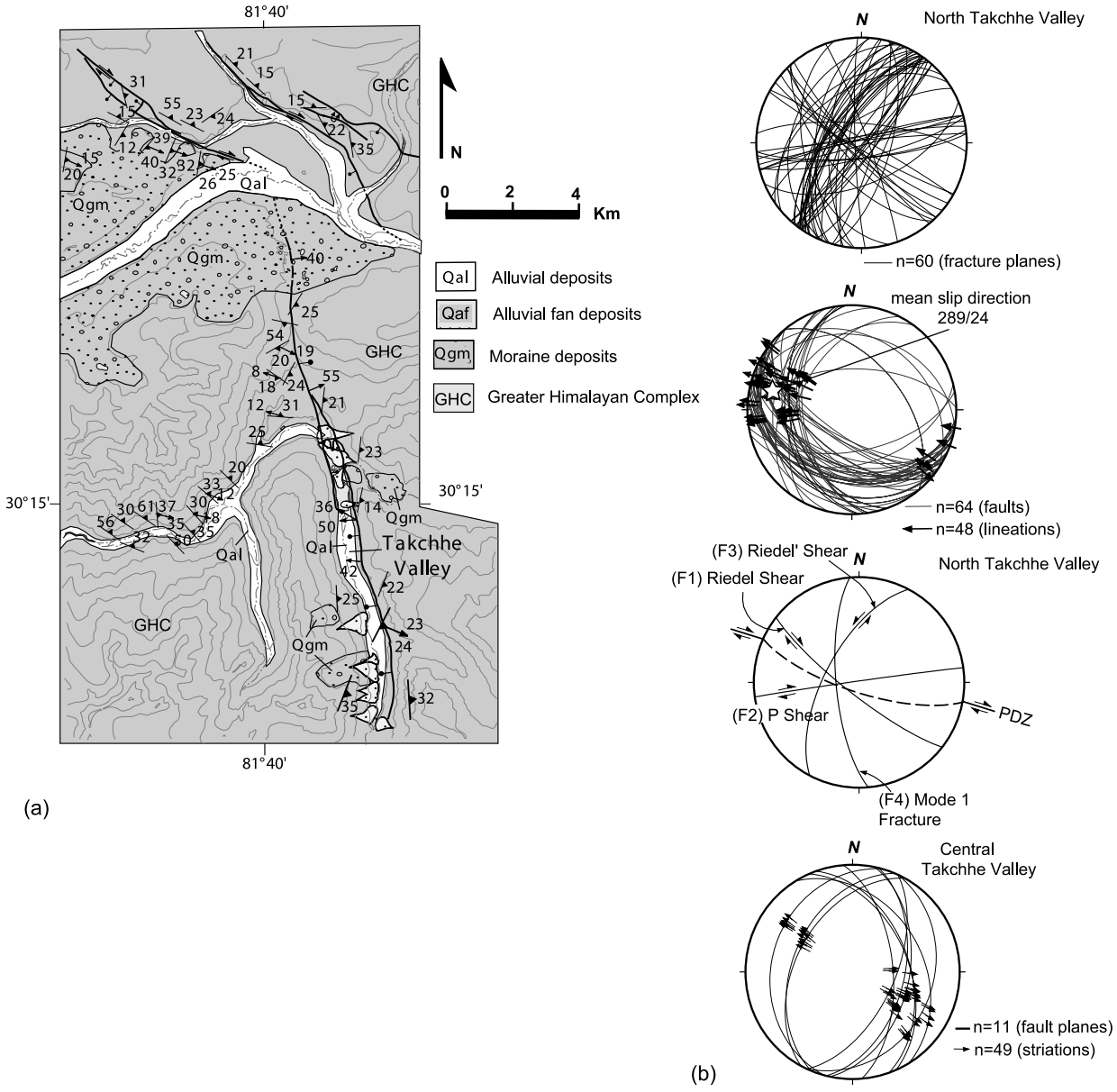

Fig. 9. Geologic map and structural data from Takchhe valley.

right-slip faults parallel older structural features such as the Tethyan fold-thrust belt and Indus–Yalu suture zone. On the other hand normal faults consistently strike north–south. Fracture and fault data in Takchhe valley shows that R′ shears and joints (Mode I fractures) share similar orientations as normal faults. Moreover, R′ shears in the Chuwa khola area display variable slip directions ranging from dominantly left-slip motion to normal dip-slip motion. We interpret that extensional stepover structures developed along R′ shears and joints. This interpretation predicts that R′ shears initiated as left-slip shear fractures and later evolved to normal dip-slip faults, possibly due to clockwise vertical axis rotation.

The active fault system broadly coincides with older ductile shear zones that are interpreted to be part of the Karakoram fault system (Fig. 11). Movement along these shear zones is estimated to be middle to late Miocene (Murphy et al., 2002; Lacassin et al., 2004; Phillips et al., 2004; Murphy and Copeland, 2005). Slip directions from ductile shear zones parallel those for the active system (Murphy et al., 2002; Murphy and Copeland, 2005). We interpret this spatial and kinematic correlation between ductile and brittle structures to represent older and younger features of the same evolving shear zone, respectively.

3.1. Timing of faulting

Nearly all lakes in Tibet display paleoshorelines that lie several tens of meters above the present lake surface. Because the fault system described in this study cuts paleoshorelines in the Mapam Yum Co area, the age of the shorelines places an upper limit on the age of fault slip. In northwestern Tibet, Avouac et al. (1996) determined a middle Holocene age

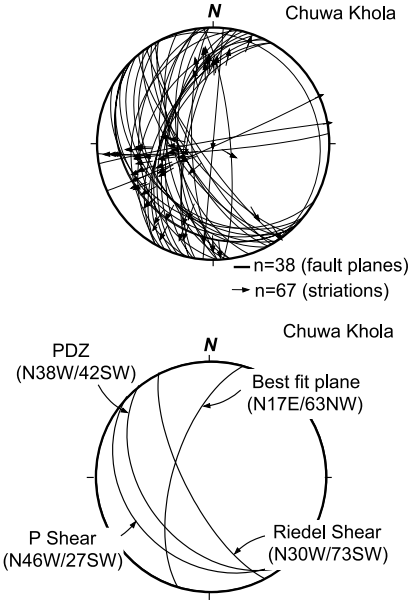

Fig. 10. Structural data from Chuwa khola.

(∼6–5.5 ka) for the highest paleoshorelines observed around Longmu Co (Fig. 1). They inferred that this age represents the end of the last glacial retreat. Precipitation in the interior of Tibet is in part a function of its distance from the Indian Ocean and its proximity to the Himalayas (e.g. Bookhagen et al., 2005). Although Longmu Co and Mapam Yum Co lie several hundred kilometers apart, both are north of the High Himalaya and are at far distances from the Indian Ocean. Because we do not suspect that the landscape has changed significantly since the middle Holocene, we infer that the age of the highest paleoshoreline at Longmu Co is the same age as that at Mapam Yum Co (Fig. 4). Brown et al. (2002) determined that the glacial advance in the Ladakh Himalaya along the central segment of the Karakoram fault occurred $\sim 90 \pm 15$ ka. Further south along strike (80°E, 32°3′N), Chevalier et al. (2005) dated two offset moraine deposits that yield mean ages of 140 ± 5.5 and 35 ± 9 kyr. Since the active Karakoram fault system within the study area cuts both paleoshorelines (Fig. 4) and glacial moraines (Fig. 6), the ages above likely represent upper bounds on the timing of the latest movement on the fault system.

3.2. Relationship between landscape and active deformation

Several major drainage basins coalesce in the Mt. Kailas area, the Brahmaputra, Karnali, Mapam Yum Co, Sutlej, and Indus (Fig. 11). The Karnali, Indus, and Sutlej rivers are transhimalayan rivers. The Brahmaputra river flows parallel to the strike of the Himalayan orogen to Namche Barwa where it then wraps around the Himalaya and drains into the Bay of Bengal. Mapam Yum Co is an internally drained basin nested within the other drainage basins. Drainage divides are determined from a digital elevation model generated from three arc second (90 m) Shuttle Radar Topography Mission

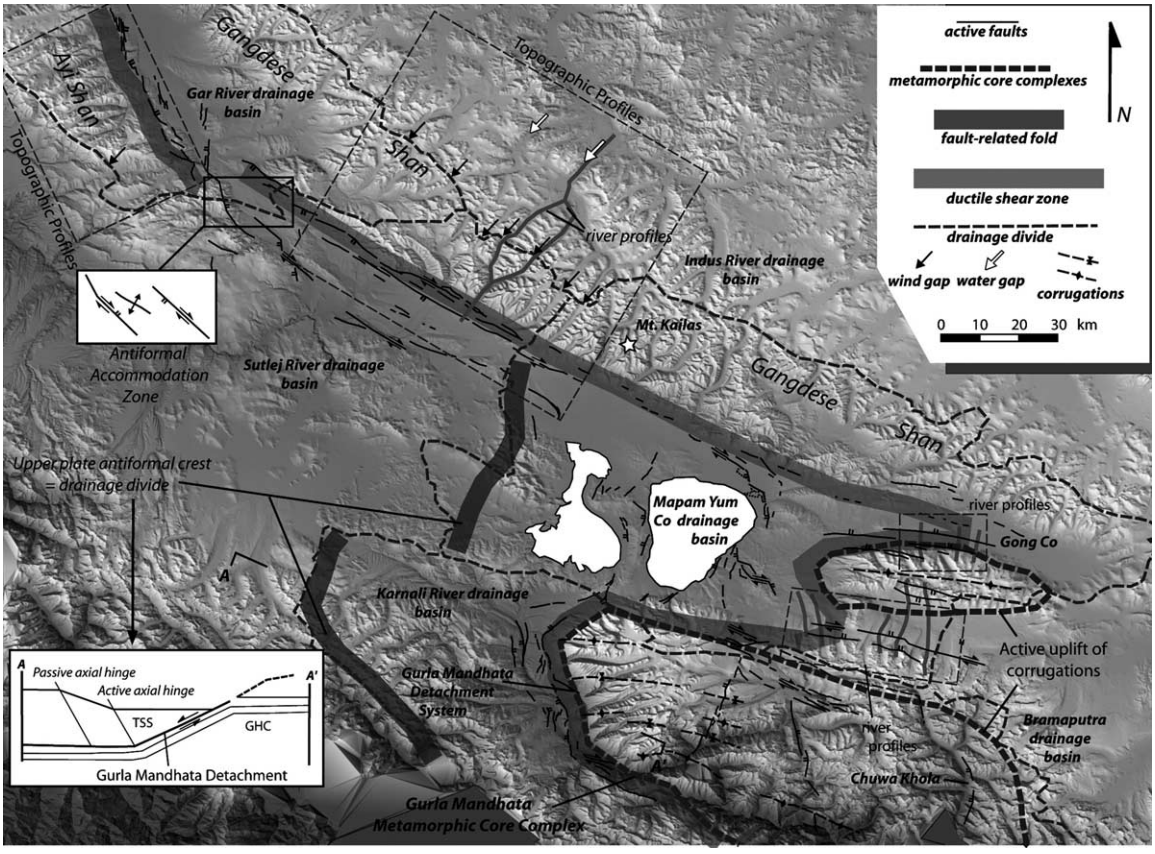

Fig. 11. Map showing the relationship between active faults, topography, river patterns, and drainage divides. Also shown is the position of ductile shear zones that correlate to older exhumed portions of the active fault system. Base map is hillshade relief generated from the SRTM DEM with a sun azimuth of 230°.

(SRTM) data. Topography is asymmetric across the Mapam Yum Co extensional stepover structure and Gurla Mandhata detachment system. To the east of these structures, the lower plate (footwall) is topographically high and the upper plate (hanging wall) is topographically low. We interpret the eastern limit and southern margins of the Mapam Yum Co drainage basin is controlled by footwall uplift by normal dip-slip motion along the Mapam Yum Co stepover structure and Gurla Mandhata detachment system. Satellite imagery of the western margin of the Mapam Yum Co drainage basin shows little active faulting. Although we do not have field data from this part of the drainage divide, we note that if the Gurla Mandhata detachment system and Mapam Yum Co stepover structure shallow at depth (ramp-flat geometry), then a hanging wall anticline would be predicted to exist west of the fault trace. It is possible that the western margin of the Mapam Yum Co and Karnali river drainage basins coincide with the crest of such a structure.

The intersection of the Karakoram fault and the Indus–Sutlej drainage divide corresponds to a position along the Karakoram fault where the master fault changes dip direction from east north of the divide to west south of the divide (Fig. 11). North of the drainage divide the Karakoram fault lies along the eastern flank of the Ayi shan. South of the drainage divide the Karakoram fault lies along the western flank of the Gangdese shan. Topographic profiles across the Ayi shan show clear asymmetry with steeper slopes along the eastern flank adjacent to the Karakoram fault (Fig. 12). Topographic trends across the Gangdese shan show an opposite asymmetry with steeper slopes along its western flank. Combined with the structural information presented above, we interpret the topographic trends are a product of elastic footwall rebound due to normal dip-slip motion along the range bounding faults (Fig. 12) (e.g. Masek et al., 1994). Between these two oppositely dipping fault segments is an elongated topographic high that trends subparallel to the faults in the overlap region. We interpret this topographic high is created by the dip-slip component of the net slip on overlapping antithetic faults (Faulds and Varga, 1998).

The geomorphology of the Gangdese and Ayi shans suggests rock uplift due to faulting is outpacing erosion. Several wind gaps in the Gangdese shan define the drainage divide between the Mapam Yum Co and Indus river drainage basins (Figs. 11 and 12). East of the drainage divide water gaps are present. Fig. 12 shows two stream profiles across the Gangdese shan. Steeper gradients are found on the west side of the range close to the Karakoram fault, while shallower gradients are on the east side of the range. The position of the wind gap defines the boundary between steep and shallow gradients. Normal dip-slip motion on the Karakoram fault predicts that the rate of bedrock uplift is greatest adjacent to the Karakoram fault and tapers off towards the east. This explains wind gaps proximal to the Karakoram fault, which imply bedrock uplift outpaced erosion, and water gaps far from the fault, which imply erosion is in pace with bedrock uplift.

East of Mapam Yum Co, active faults flank both sides of two metamorphic core complexes (Fig. 11). Offset glacial moraine deposits, sag ponds, and beheaded streams show right-lateral separations. Bedrock stream profiles along the flanks of the metamorphic core complexes show a step-shaped geometry (Fig. 13). We calculated stream length–gradient (SL) indices along these profiles. The SL index is a hydrologic variable related to the ability of a stream to erode its bed and transport sediment (Keller and Pinter, 2002). It is sensitive to changes in channel slope and is used to evaluate possible tectonic activity and changes in rock resistance. Segments of streams that have high SL indices correlate to lineaments that we interpret as active faults (Fig. 13). The fault geometry and kinematics are

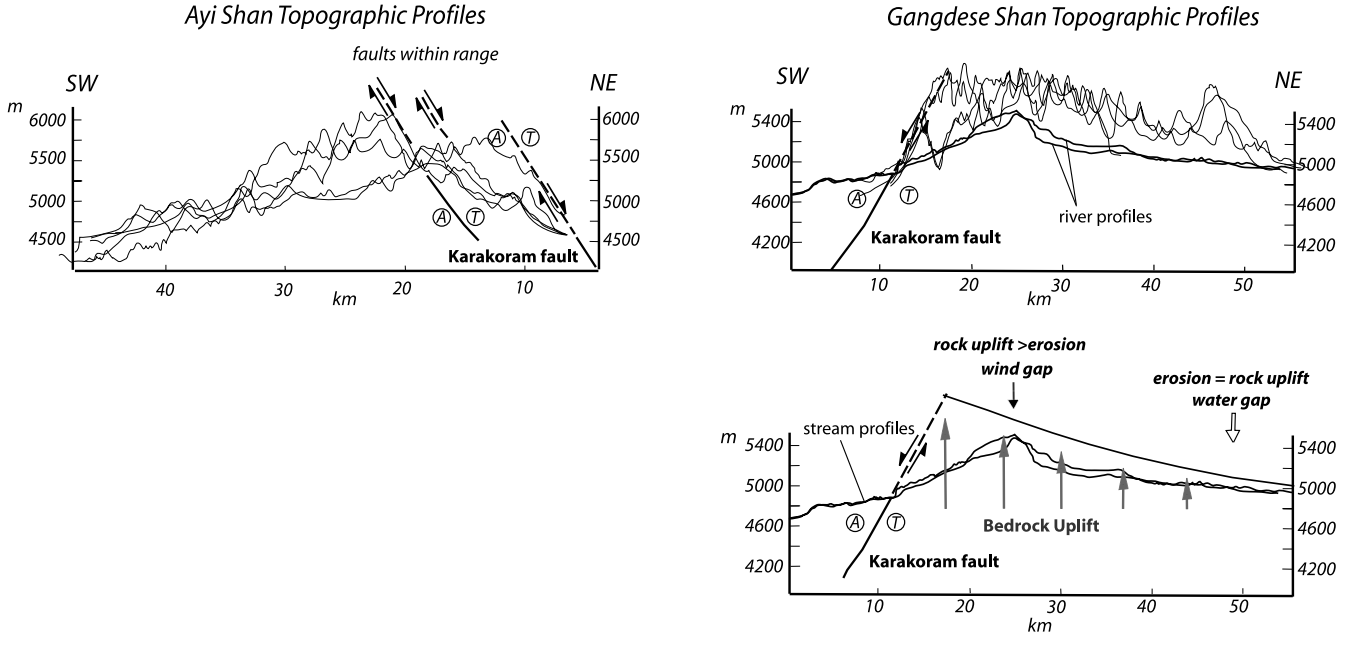

Fig. 12. Topographic profiles across the Ayi shan and Gangdese shan. Location of topographic profiles is shown on Fig. 11. Profiles are generated from SRTM data. The geomorphology of the ranges is interpreted to result from normal right-slip motion along the south side of the Gangdese shan and north side of the Ayi shan.

consistent with uplift of the two metamorphic core complexes. Because the core complexes are regional antiformal corrugations in the footwall of the Gurla Mandhata detachment system (Murphy et al., 2000; Murphy and Copeland, 2005), we suggest they are actively growing and accommodate north–northwest shortening within the transtension zone.

3.3. Transtension zone geometry and kinematics

In the Mt. Kailas area between 81°E and 82°E the zone of transtensional deformation is ~90 km wide and bordered on the north by the Gangdese range and the region immediately south of the Gurla Mandhata–Humla fault system on the south (Fig. 14). These boundaries are subparallel, strike ~120°, and the transport direction is oblique. The geometry and kinematics of brittle structures and corrugations are consistent with wrench-dominated transtension. Simple shear within the zone is accommodated by right-lateral R and P shears as well as left-lateral R′ shears. The mean orientation of Mode 1 fractures is 355° resulting in an instantaneous stretching direction of 085° and a transport direction across the transtension zone of 102.5°, $\alpha = 72.5°$, where α is defined as the angle between the zone orthogonal and the transport direction, or $\alpha = 252.5°$ using the convention of Dewey (2002). Vertical shortening is accommodated by ~north-striking normal faults and horizontal shortening is accommodated by ~east–west-trending corrugations. Taylor et al. (2003) show that north–south shortening of the Tibetan plateau can be explained by conjugate strike-slip

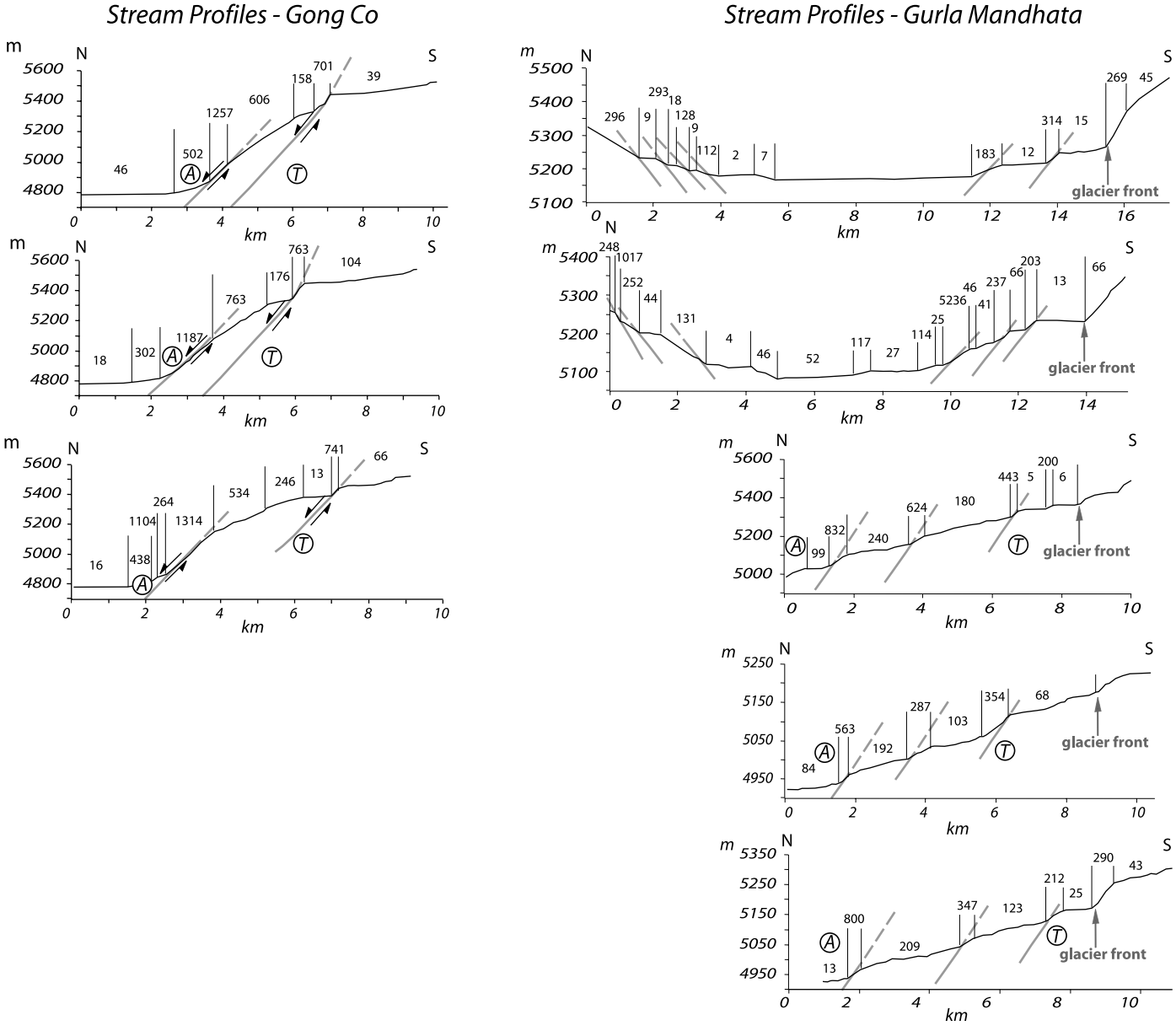

Fig. 13. Stream profiles located along flanks of metamorphic core complexes. See Fig. 11 for location. Profiles were extracted from an SRTM DEM. Numbers along profiles are Stream length–gradient indices (SL). SL = $(\Delta H/\Delta L)^*L$, where ΔH is the change in elevation of the reach, ΔL is length of the reach, and L is the total channel length from the midpoint of the reach to the highest point on the channel. Regions with high SL indices correlate to lineaments we interpret as faults.

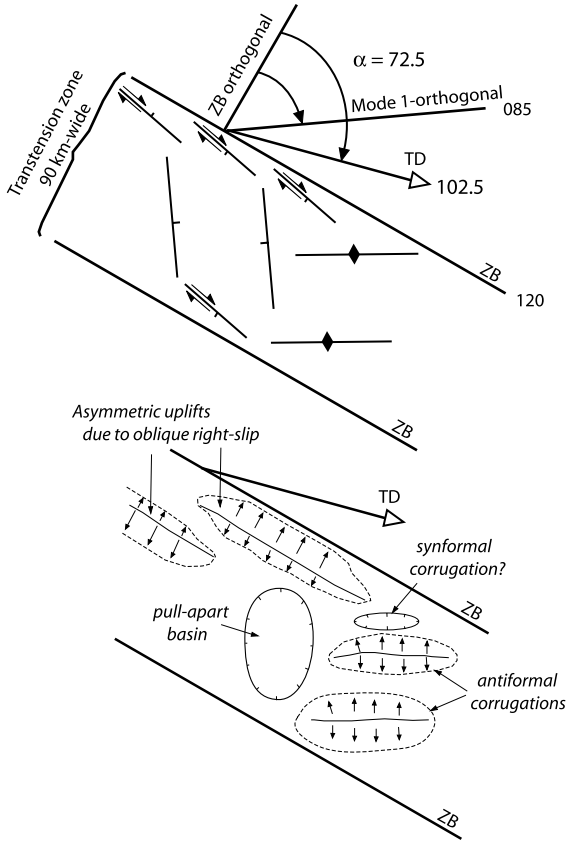

Fig. 14. (A) Model describing active noncoaxial dominated dextral transtension along the Karakoram fault system. ZB, zone boundary; TD, transport direction. (B) Schematic representation of the geomorphology. Arrows indicate slope direction, dashed lines designate uplifts, and lines with ticks are depressions.

faulting. Our data suggest that transtension-related corrugations also need to be considered in shortening estimates across the Tibet–Himalayan collision zone.

4. Conclusions

Geologic and geomorphologic observations from southwest Tibet and northwest Nepal, in the vicinity of Mt. Kailas support the following aspects regarding the nature of active deformation along the Karakoram fault:

(1) The geometry and kinematics of active deformation indicates wrench-dominated transtension distributed over a 90-km-wide zone striking 120° with a transport direction across the zone = 102.5°. Simple shear within the zone is accommodated by right-lateral R and P shears as well as left-lateral R′ shears. Vertical shortening is accommodated by ~north-striking normal faults and north–northwest oriented shortening is accommodated by ~east–west-trending transtension-related corrugations.
(2) Drainage divides strike both at high angles and subparallel to the transtension zone. We interpret that drainage divides that strike at a high angle to the zone are controlled by movement along north-striking extensional fault systems and drainage divides subparallel to the zone are controlled by uplift of corrugations as well as uplift due to oblique movement along right-slip faults.

Acknowledgements

This research was supported by National Science Foundation grant EAR-0106808. Additional support was provided by the University of Houston GEAR program. Early versions of this manuscript benefited greatly by reviews from Robert Holdsworth, Mike Edwards, and Mike Searle as well as discussions with Mike Taylor.

References

Armijo, R., Tapponnier, P., Han, T., 1989. Late Cenozoic right-lateral strike-slip faulting in southern Tibet. Journal of Geophysical Research 94, 2787–2838.

Avouac, J.-P., Tapponnier, P., 1993. Kinematic model of active deformation in central Asia. Geophysical Research Letters 20, 895–898.

Avouac, J.-P., Dobremez, J.-F., Bourjot, L., 1996. Palaeoclimatic interpretation of a topographic profile across middle Holocene regressive shorelines of Longmu Co (Western Tibet). Palaeogeography, Palaeoclimatology, Palaeoecology 120, 93–104.

Bookhagen, B., Thiede, R.C., Strecker, M.R., 2005. Late Quaternary intensified monsoon phases control landscape evolution in the northwest Himalaya. Geology 33, 149–152.

Brown, E.T., Bendick, R., Bourlès, D.L., Gaur, V., Molnar, P., Raisbeck, G.M., Yiou, F., 2002. Slip rates of the Karakoram fault, Ladakh, India, determined using cosmic ray exposure dating of debris flows and moraines. Journal of Geophysical Research 107, 71–713.

Cheng, J., Xu, G., 1987. Geologic map of the Gerdake region at a scale of 1:1000000 and geologic report. Xizang Bureau of Geology and Mineral Resources, 363pp. (in Chinese).

Chevalier, M.-L., Ryerson, F.J., Tapponnier, P., Finkel, R.C., Van Der Woerd, J., Li, H., Liu, Q., 2005. Slip-rate measurements on the Karakoram fault may imply secular variations in fault motion. Science 307, 411–414.

Dewey, J.F., 2002. Transtension in arc and orogens. International Geology Review 44, 402–439.

Dewey, J.F., Holdsworth, R.E., Strachan, R.A., 1998. Transpression and transtension zones. In: Holdsworth, R.E., Strachan, R.A., Dewey, J.F. (Eds.), Continental Transpressional and Transtensional Tectonics. Geological Society, London, Special Publications, vol. 135, pp. 1–14.

Faulds, J.E., Varga, R.J., 1998. The role of accommodation zones and transfer zones in the regional segmentation of extended terranes. Geological Society of America Special Paper 323, 1–45.

Fossen, H., Tikoff, B., 1998. Extended models of transpression and transtension, and application to tectonic settings. In: Holdsworth, R.E., Strachan, R.A., Dewey, J.F. (Eds.), Continental Transpressional and Transtensional Tectonics. Geological Society, London, Special Publications, vol. 135, pp. 15–33.

Jade, S., Bhatt, B.C., Yang, Z., Bendick, R., Gaur, V.K., Molnar, P., Anand, M.B., Kumar, D., 2004. GPS measurements from the Ladakh Himalaya, India: preliminary tests of plate-like or continuous deformation in Tibet. Geological Society of American Bulletin 116, 1385–1391.

Kapp, P., Guynn, J.H., 2004. Indian punch rifts Tibet. Geology 32, 993–996.

Kapp, P., Murphy, M.A., Yin, A., Harrison, T.M., 2003. Mesozoic and Cenozoic tectonic evolution of the Shiquanhe area of western Tibet. Tectonics 22. doi:10.1029/2001TC001332.

Keller, E.A., Pinter, N., 2002. Active Tectonics: Earthquakes, Uplift, and Landscape, Second Edition: Upper Saddle River. Prentice Hall, New Jersey. 362pp.

Lacassin, R., Valli, F., Arnaud, N., Leloup, P.H., Paquette, J.L., Li, H., Tapponnier, P., Chevalier, M.-L., Guillot, S., Maheo, G., Xu, Z., 2004. Large-scale geometry and offset of the Karakoram fault, Tibet. Earth Planetary Science Letters 219, 255–269.

Larson, K.M., Burgmann, R., Bilham, R., Freymueller, J.T., 1999. Kinematics of the India–Eurasia collision zone from GPS measurements. Journal of Geophysical Research 104, 1077–1093.

Masek, J.G., Isacks, B.L., Fielding, E.J., Browaeys, J., 1994. Rift-flank uplift in Tibet: evidence for crustal asthenosphere. Tectonics 13, 659–667.

Murphy, M.A., Copeland, P., 2005. Transtensional deformation in the central Himalaya and its role in accommodating growth of the Himalayan orogen. Tectonics 24. doi:10.1029/2004TC001659.

Murphy, M.A., Yin, A., Kapp, P., Harrison, T.M., Ding, L., Guo, J., 2000. Southward propagation of the Karakoram fault system, southwest Tibet. Timing and magnitude of slip. Geology 28, 451–454.

Murphy, M.A., Yin, A., Kapp, P., Harrison, T.M., Manning, C.E., 2002. Structural and thermal evolution of the Gurla Mandhata metamorphic core complex, southwest Tibet. Geological Society of America 114, 428–447.

Ni, J., Barazangi, M., 1984. Active tectonics of the western Tethyan Himalaya above the underthrusting Indian plateau: the upper Sutlej river basin as a pull-apart structure. Tectonophysics 112, 277–295.

Norris, R.J., Koons, P.O., Cooper, A.F., 1990. The obliquely-convergent plate boundary in the South Island of New Zealand: implications for ancient collision zones. Journal of Structural Geology 12, 715–725.

Oldow, J.S., Aiken, C.L.V., Hare, J.L., Ferguson, J.F., Hardyman, R.F., 2001. Active displacement transfer and differential block rotation within the central Walker Lane, Great Basin. Geology 29, 19–22.

Phillips, R., Parrish, R.R., Searle, M.P., 2004. Age constraints on ductile deformation and long-term slip rates along the Karakoram fault zone, Ladakh. Earth and Planetary Science Letters 226, 305–319.

Ratschbacher, L., Frisch, W., Liu, G., 1994. Distributed deformation in southern and western Tibet during and after the India–Asia collision. Journal of Geophysical Research 99, 19917–19945.

Replumaz, A., Tapponnier, P., 2003. Reconstruction of the deformed collision zone between India and Asia by backward motion of lithospheric blocks. Journal of Geophysical Research 108. doi:10.1029/2001JB000661.

Rothery, D.A., Drury, S.A., 1984. The neotectonics of the Tibetan plateau. Tectonics 3, 19–26.

Searle, M.P., 1996. Geological evidence against large-scale pre-Holocene offsets along the Karakoram fault: implications for the limited extrusion of the Tibetan plateau. Tectonics 15, 171–186.

Searle, M.P., Weinberg, R.F., Dunlap, W.J., 1998. Transpressional tectonics along the Karakoram fault zone, northern Ladakh: constraints on Tibetan extrusion. In: Holdsworth, R.E., Strachan, R.A., Dewey, J.F. (Eds.), Continental Transpressional and Transtensional Tectonics. Geological Society, London, Special Publication, vol. 135, pp. 307–326.

Taylor, M., Yin, A., Ryerson, F.J., Kapp, P., Ding, L., 2003. Conjugate strike-slip faulting along the Banggong–Nujiang suture zone accommodates coeval east–west extension and north–south shortening in the interior of the Tibetan plateau. Tectonics 22. doi:10.1029/2002TC001361.

Tikoff, B., Teyssier, C., 1994. Strain modeling of displacement field partitioning in transpressional orogens. Journal of Structural Geology 16, 1575–1588.

Wang, Q., Zhang, P., Freymueller, J., Bilham, R., Larson, K., Lai, X., You, X., Niu, Z., Wu, J., Li, Y., Wang, Z., Chen, Q., 2001. Present-day crustal deformation in China constrained by Global Positioning System measurements. Science 294. doi:10.1126/SCIENCE.1063647.

Yin, A., Harrison, T.M., 2000. Geologic evolution of the Himalayan–Tibetan orogen. Annual Reviews of Earth and Planetary Science 28, 211–280.

Zhang, J., Ding, L., Zhong, D., Zhou, Y., 2000. Orogen-parallel extension in the Himalaya: is it the indicator of collapse or the product in process of compressive uplift? Chinese Science Bulletin 45, 114–119.

Zhang, P.-Z., Shen, Z., Wang, M., Gan, W., Bürgmann, R., Molnar, P., Niu, Z., Sun, J., Wu, J., Hanrong, S., Xinzhoa, Y., 2004. Continuous deformation of the Tibetan plateau from global positioning system data. Geology 32, 809–812.